IOP Conf. Series: Materials Science and Engineering **249** (2017) 012018 doi:10.1088/1757-899X/249/1/012018

Flows due to pressure induced dissociation-formation of gas hydrates

J R Agudo[1], S Kwon[1], R Saur[1], S Loekman[2], G Luzi[1], C Rauh[3], A Wierschem[4] and A Delgado[1,4]

[1]Institute of Fluid Mechanics, FAU Busan Campus, University of Erlangen-Nuremberg,
46-742 Busan, Republic of Korea
[2]Institute of Chemical Reaction Engineering, FAU Busan Campus, University of Erlangen-Nuremberg,
46-742 Busan, Republic of Korea
[3]Department of Food Biotechnology and Food Process Engineering
Technische Universität Berlin
D-14195 Berlin, Germany
[4]Institute of Fluid Mechanics, University of Erlangen-Nuremberg,
D-91058 Erlangen, Germany

Antonio.delgado@fau.de

Abstract. During the last decade, Gas Hydrates (GH) have attracted the interest of the scientific community for engineering applications. Carbon dioxide hydrate (CO_2H), for instance, may play an important role for capture and sequestration methods in order to reduce global climate change. Despite the extensive literature, the transport phenomena involved during CO_2H formation are not yet fully understood. CO_2 transfer from gas or liquid phase to the bulk of water is expected to happen not only by molecular diffusion but also driven by natural convective currents induced by CO_2 dissolution in water. Using particle tracer methods, we experimentally characterize the flow velocity of the bulk of water during CO_2H formation. For that purpose, CO_2H is grown inside an optical cell with a volume of 12 mL at various pressures and temperatures. Due to CO_2 dissolution, convection currents are noticed prior to hydrate formation. Our experimental results point to a significant correlation between this process and the subsequent hydrate formation. Two well-differentiated hydrate growth patterns were observed depending on the hydrate induction time and the corresponding CO_2 concentration distribution inside water. For long induction times, CO_2 can be provided from the water phase resulting in rapid growth. Short induction times resulted in slow growth at the interface creating a solid barrier accompanied by a significant drop in the flow velocity. In some cases, the hydrate layer appeared to be unstable and convection could restart.

1. Introduction

Gas Hydrates (GHs) are crystalline solids consisting of gas molecules, also called guest or former molecules, enclosed in water cavities composed of hydrogen-bonded water molecules, also referred as host molecules [1]. Methane, ethane, propane or CO_2 are typical sorts of gas hydrate former. There is no bonding between frozen water and former gas molecules which are free to rotate inside the frozen water cage. The stabilization resulting from gas molecule is supposed to be due to van der Waals forces

(attraction forces between molecules) and hydrogen bonds [2]. Given the enormous amounts of methane enclosed in form of hydrate that is encountered in deep ocean floors [3], Methane Hydrates (MHs) are considered as one of the most important future source of hydrocarbon fuel [4].

Unlike MH, the existence of CO_2 Hydrates (CO_2Hs) as permanent disposal in Earth seems to be unrealistic as experimentally observed by [5]. However, CO_2H is assumed to be abundant in the solar system playing a potential role in shaping the Martian landscape [6], or as a source of potable water for future human habitation [7]. Coming back to earthling applications, CO_2H formation-dissociation processes have recently attracted the interest of the scientific community for bioenergy applications. They are, for instance, of vital importance for CO_2 capture and sequestration methods, known as CCS. CCS are considered as one of the potential ways to reduce global climate change by preventing CO_2 gas emissions to the atmosphere. The first step of this process consists of separating CO_2 gas from exhaust emissions, coming for instance from fossil fuel power plants [8, 9]. Here, hydrated-base CO_2 separation points to a very promising alternative to current methods, e.g. absorption, adsorption, membrane separation or cryogenic fractionation [9, 10, 11, 12]. The last step of CCS process is the CO_2 storage into a safe and long-term system. Here, sequestering a large amount of CO_2 into deep ocean set-up has been recently contemplated in literature. The replacement of CO_2 in marine MH deposits would permit CO_2 storage and release of methane as energetic input at the same time [9, 13]. Other novel industrial applications include CO_2H-based water desalinization [14, 15, 16] or CO_2H-based liquid concentration process for the food industry [17, 18]. To find a reliable, reproducible and efficient experimental method for GH production-dissociation process, is crucial for studying its viability in the aforementioned applications.

Despite the extensive literature, the transport phenomena involved during CO_2H formation are not yet fully understood. CO_2 transfer from gas or liquid phase to the bulk of water, for instance, is expected to happen not only by molecular diffusion but also driven by natural convective currents induced by CO_2 dissolution in water [19, 20, 21]. These currents, that might play a key role in the CO_2 transport prior to hydrate formation, have not considered yet in classical mass transport models for CO_2H formation. Using particle tracer methods, we experimentally characterize the flow velocity of the bulk of water during CO_2H formation. For that purpose, CO_2H is grown inside an optical cell with a volume of 12 mL at various pressures and temperatures. Due to CO_2 dissolution, convection currents are noticed prior to hydrate formation. Our experimental results point to a significant correlation between this process and the subsequent hydrate formation.

2. Experimental set-up

CO_2H is formed in a cylindrical optical cell with a total volume of 12 mL, and dimensions of 25 mm in height and diameter, designed for pressures up to 350 bars. The pressure cell contains four sapphire glasses for optical access and a cooling jacket to keep the temperature constant at 273.5 ± 0.5 K with the help of a circulating bath. The temperature is controlled with a K-type thermocouple coupled to the center of the cylindrical cell. The pressure is continually recorded outside the reactor by a pressure transducer within a relative uncertainty lower than 1%. Figure 1 illustrates the optical cell used for the experiments.

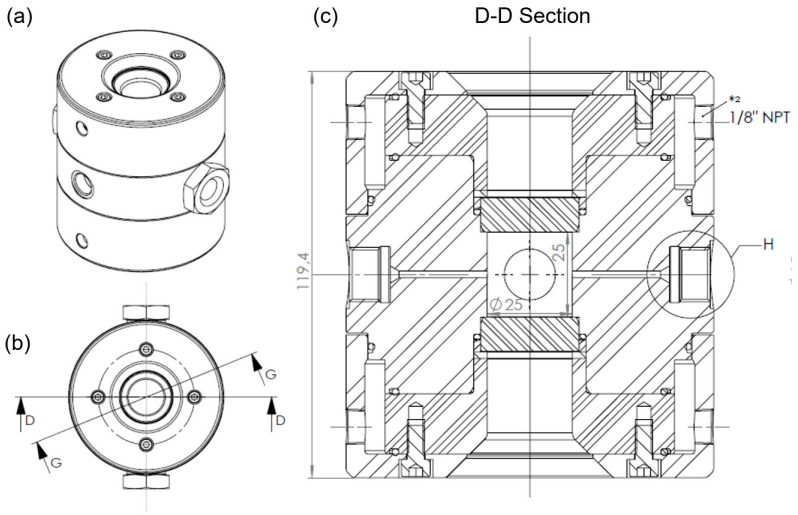

Figure 1. Optical cell with a volume of 12 mL and a total of four sapphire glasses used for the experiments (a). Top view (b) and vertical sectional view (c). The measurements are shown in mm.

To form CO_2H, 5.5 or 7 mL of deionized water (18.2 MΩ X cm of resistivity) are added first to the optical cell. After flushing the system, high purity CO_2 (99.95%) is injected into the vessel to achieve the proper pressure to form hydrate. Two different pressures were selected to form hydrate, 36 and 56 bars. The former is the equilibrium pressure between gaseous and liquid CO_2 at the operating temperature. Under this pressure, there are three phases in the reactor prior to hydrate formation: liquid water, liquid CO_2, and gaseous CO_2 from the bottom to the top in the reactor. The latter pressure corresponds to the maximum provided by the CO_2 bottle at the same temperature. In this case, only liquid water and liquid CO_2 are encountered in the reactor before hydrate formation.

To characterize the flow in the bulk of water, the water is seeded with Polyamide Seeding Particles (PSP-5) of 5 microns diameter with a density of 1030 kg/m^3. At operating conditions, the settling velocity of PSP remains about 3 order of magnitude smaller than typical velocities due to buoyancy driven convection flows at onset of experiment. Given the long-term duration of the experiments, up to 48 hours for hydrate formation, a continuous cold LED source of 55 W with a light guide of 15 mm in diameter is selected for the volume illumination of the cell. The use of this low power light source showed a marginal impact on the bulk temperature and allows us to continue the particle image velocimetry (PIV) measurements in the bulk of water once the hydrate growths in the interface. Two different imaging systems are simultaneously used for conducting the measurements. A 1280 x 1024 CMOS camera coupled to a 180 mm, f/3.5 Macro lens is used for recording from the front at a working distance of 730 mm from the center of the cylindrical cell. The field of view, in this case, is a circular window of 15 mm in diameter which corresponds to the dimensions of the sapphire glass integrated into the side of the reactor. A 1920 x 1080 CMOS camera equipped with a modular zoom lens system that incorporates a tilted mirror is used for recording from the back. The working distance is 53 mm. The magnification of the lens system ranges between M = 1.1 and M = 7.8, and the numerical aperture between NA = 0.036 and NA = 0.12, respectively. The field of view ranges between 4.2 x 5.6 and 0.61 x 0.81 mm, while the depth of field ranges between 0.42 and 0.038 mm, respectively. Figure 2 illustrates the experimental set-up. While the front camera is used to measure the flow velocity in the entire bulk of water (see Figure 3), the back camera permits us to focus on the interface, where hydrate formation is likely to happen (see Figure 4). For the front and the back system, the images are recorded at a video rate of 2 and 5 Hz, respectively. The particle image fields are analyzed by classical cross-correlation implemented by fast Fourier transform using Insight4G®. The size of the interrogation area is 32 x 32

pixels in both systems. This corresponds to a spatial resolution of approximately 0.4 mm in the front system. Defining a peak to noise peak ratio of 1.47, the analyzed particle-image fields reveal typical ratios of good vectors above 80%. The PIV analysis, however, produces a few obvious false positive velocities vectors which are several orders of magnitudes larger than the average. Additionally, all points outside of the processing mask are zero. Thus, to remove the false positive values every point with a velocity above the 95%-tile of non-zero velocities was cut. When calculating the average velocity at a specific point in time, only non-zero velocities were considered. In order to improve readability, the velocities were averaged over 30 seconds.

The accuracy of the PIV system installed in the back was checked with the known solution of a Couette flow velocity profile induced by an MCR302 rotational rheometer with a parallel-disk configuration. A circular container with transparent Plexiglas sidewalls and a chamfer in the front was concentrically coupled to the rheometer. For more details in this experimental set-up, we refer to [22, 23]. The distance from the rotating plate to the surface is fixed at 2 mm and the angular frequency of the rotating plate was set to obtain velocities of the order than those observed during GH formation experiments. The PIV measurements revealed a deviation lower than 5% with respect to the expected flow velocity confined between the plates. A comparison in velocity between the front and the back PIV system showed typical deviations lower than 10%.

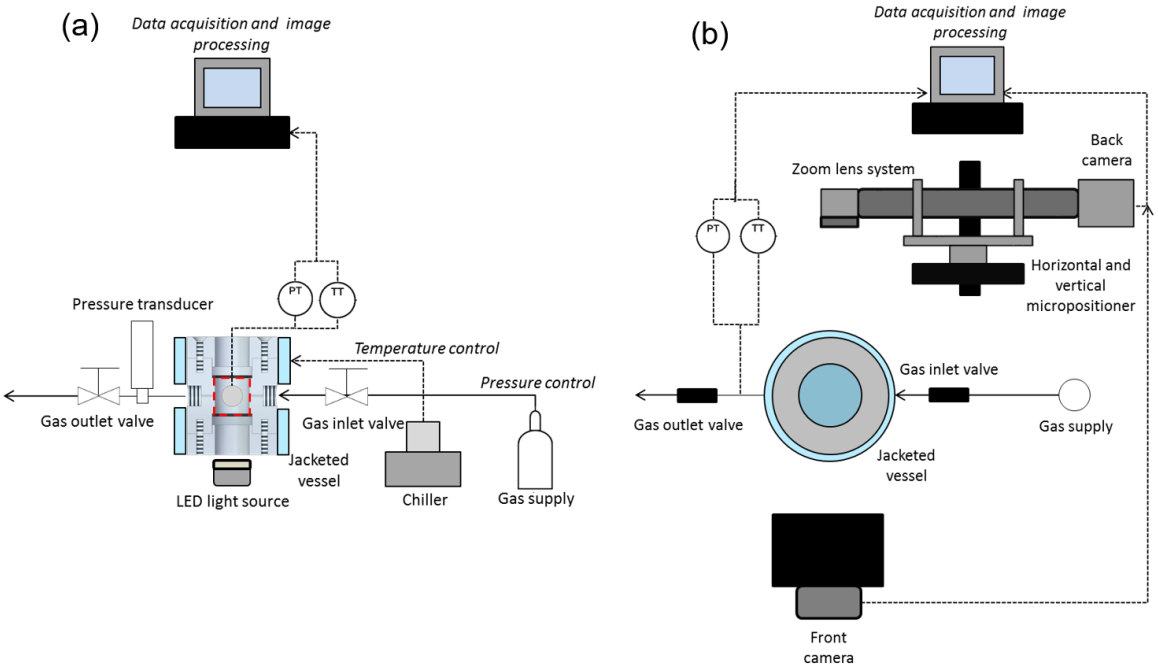

Figure 2. Sketch of the experimental set-up for PIV measurements during CO_2 hydrate formation. Front view (a) and top view (b).

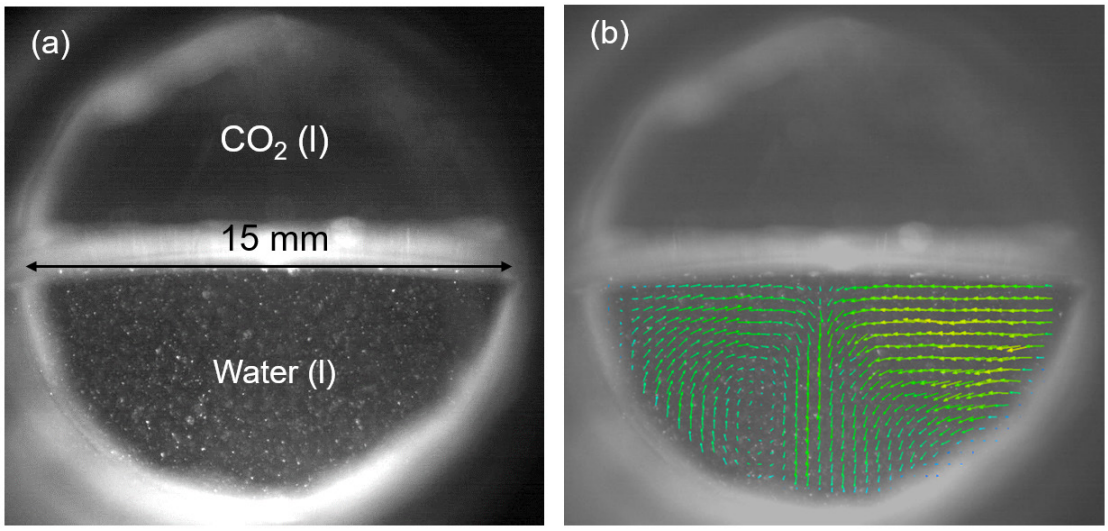

Figure 3. Digital image of the seeded flow inside the optical cell recorded from the front imaging system at 56 bar and 273.5 K (a). Velocity vector map obtained by the aforementioned system prior to hydrate formation (b).

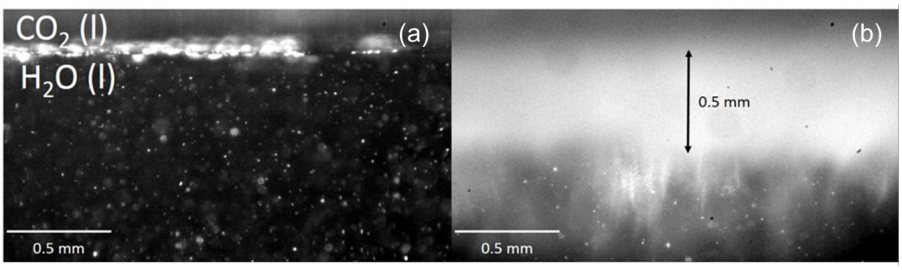

Figure 4. Digital image of the seeded flow inside the optical cell recorded from the back imaging system at 56 bars and 273.5 K prior to hydrate formation (a). Frame representing the onset of hydrate formation in the experiment (b).

3. Results and discussion

In a system as shown in Figure 3, CO_2 is first expected to dissolve into the water phase by molecular diffusion through the interface [20]. Since the dissolution of CO_2 increases the density of water [24], a gradient of density is expected to induce the instability of the boundary layer saturated with CO_2 [19, 20]. This instabilities yields in recirculation flow as shown in Figure 3(b). The criteria to predict the existence of this natural convection is usually characterized by the Rayleigh number, which depends on the fluid properties and geometry dimensions. The Rayleigh number can be defined as [20, 21]:

$$Ra = \frac{\Delta\rho g R^3}{\rho_i \nu D} \tag{1}$$

where $\Delta\rho$ is the density difference of the fluid, g is the gravity acceleration, R is the radius of the cylindrical cell, ρ_i is the initial density of water, ν is the kinematic viscosity of water and D is the diffusion coefficient of water. Natural convection typically occurs when Ra>2100 [21]. The other independent dimensionless number that governs the flow is the Re numbers defined as:

$$\mathrm{Re} = \frac{uR}{\nu} \tag{2}$$

where u is the maximum in-plane velocity registered by the PIV system. At similar pressure conditions than in our experiments, gradients of density driven by CO_2 dissolution up to 8 kg/m^3 has been reported in literature [21]. Accordingly, Rayleigh numbers of the order of 10^7 are expected in our system, and buoyancy-driven convection is likely to happen prior to hydrate formation in the reactor. On the other hand, with maximum measured velocities of about 0.3 mm/s, the Reynolds number remains about 2 in our experiments indicating the existence of laminar flows.

3.1. Effect of seeding tracers on the Gas Hydrate formation

Particle image velocimetry relies on light scattering particles being suspended in the water phase. The flow velocity measurement inadvertently introduces small particles that may cause hydrate to nucleate faster as observed in other recent experiments with suspended particles [25, 26]. To investigate this possibility, experiments without seeding and with two different kinds of tracers, Silver Coated Hollow Glass Spheres 10 μm (S-HGS-10) and Polyamide Seeding Particles 5μm (PSP-5), are conducted. The experiments are compared in terms of induction time and growth pattern. At saturated conditions, we performed a total of 12 experiments with 5.5 mL of water; 3 experiments with non-seeded water, 4 experiments with PSP-5 tracers and 5 experiments with S-HGS-10 tracers. The stochastic nature of the crystallization phenomenon yielded to a broad range of induction times. In the case of trials carried out without tracers or with PSP-5 tracers, the induction time ranged between 2 and 10 hours with exception of a single with PSP-5 tracers event that took 27 hours to nucleate. In the case of experiments performed with S-HGS-10 tracers, however, the nucleation occurred in less than 15 min in all of the cases. While the induction time of experiments with PSP-5 tracers scattered similarly to experiments without tracers, experiments done with S-HGS-10 tracer showed almost immediate growth. This fact suggests that S-HGS-10 particles act as nucleation spots.

This is further corroborated, by the way hydrate nucleated inside the optical cell. In all the cases, experiments with PSP-5 seeding particles showed the typical growth from the water-former interface, as one would expect in the absence of any contaminants (see Figure 5(a)-(d)). The same nucleation pattern happening at the interface was indeed observed in experiments with non-seeded water. On the other hand, in all the experiments conducted, hydrate grew from all over the reactor when 10 micrometer-sized particles were used (see Figure 5(e)-(g)). Nucleation seems to happen in the bulk of water but also in the reactor walls as can be observed in Figure 5(e).

Given that the two types of particles are different in size and material it is not clear what caused the difference in behavior. Literature indicates that the larger size of suspended particles has a shortening effect on the induction time [26]. However, in that case, the pertinent size is that of the agglomerates, and it is not clear whether the size itself or some underlying property of the particles that caused the larger size is to blame for the lower induction lag. Furthermore, was it suggested by [26] that the functional oxide group was essential and [25] reported that suspended silver nanoparticles had no effect on the induction time. Literature seems to be lacking studies, investigating the effect of suspended particles in the micrometer range on hydrate formation. This task, however, remains out of the scope of the present study that relies on the characterization of the flow velocity prior to hydrate formation. Any further experiments were done using the Polyamide particles, where no significant difference with non-seeded experiments was observed in the induction time, nor in the growth pattern.

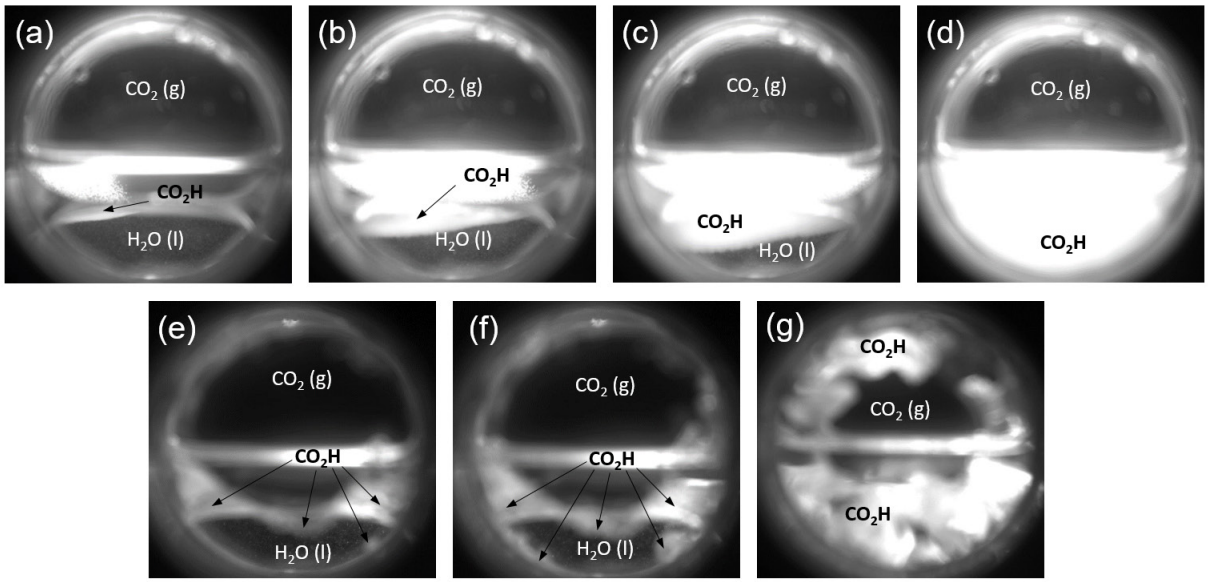

Figure 5. Snapshots illustrating the CO_2H formation with PSP-5 tracers at the interface (a)-(d) and CO_2H formation with S-HGS in the bulk of water and at the walls of the reactor (e)-(g). Experiments performed with 5.5 mL of water and CO_2 at 36 bars and 273.5 K. The induction time of hydrate formation was 2 h and 23 minutes (a) and 3 minutes (e), respectively. The time elapsed between (a) and (d) is about 5 seconds. The time elapsed between (e) and (g) is about 10 minutes.

3.2. Buoyancy-driven convection inducing flow currents prior to Gas Hydrate formation

Two preliminary experiments were conducted to clarify that buoyancy-driven convection due to CO_2 dissolution is the main cause of induced-flow currents before hydrate is formed in the optical cell. In a first experiment, once the operating temperature is achieved, CO_2 is injected into the reactor to an initial pressure of 32 bars. Pressure, temperature and averaged velocities in the bulk of water are recorded simultaneously. Figure 6 depicts the results. The data are plotted up to 6 hours. No hydrate formation was noticed during that time in this experiment. Pressure and average velocity experience a gradually decrease with time until a plateau at about 5 hours is reached. The temperature increases by approximately 1 K as a consequence of the augment in pressure. Unlike the long-term decrease of pressure with time, the measured temperature reaches a constant plateau after approximately 1 min, and keep constant during the rest of the experiment (see inset of Figure 6(a)). Since the temperature remains constant, the pressure drop in the system is mainly due to CO_2 dissolution in water [27].

Comparison between pressure and velocity trends show a remarkable similarity between each other. This indicates that CO_2 dissolving in the bulk of water but not fluctuations in temperature is the main source of the density-driven natural convection phenomenon. Note that a constant pressure in the system indicates that CO_2 is fully distributed in the bulk of water at the corresponding pressure and temperature. No gradient of CO_2 concentration exists in the bulk of water, and convection currents disappear as shown in Figure 6(b).

To check that flow velocities in the bulk of water are not driven by mechanical agitation after an increase of pressure, a second experiment is conducted by injecting water non-soluble gas helium (He) up to 56 bars at operating temperature. Open symbols in Figure 7 represent the averaged flow velocity as a function of time. Solid symbols depict the averaged velocity for an experiment performed with CO_2 at same conditions. The experiment performed with CO_2 reveals again a gradual decrease of velocity until a plateau at a marginal velocity is achieved after about 5 hours. The averaged velocity in the experiment conducted with He drops to the same value but immediately after the pressure is increased in the optical cell. The pressurization and the corresponding velocity measurements for the experiment

performed with He can be seen in Figure 7(b) and (c), respectively. The red line indicates the instant in which pressure is increased in the system. From Figure 7(c) it is clear that although increasing the pressure induces some initial movement, the effect dies down after a few seconds. This corroborates that without the dissolution-driven Rayleigh convection the measured velocities are significantly lower. Note that convection induced by a temperature gradient should still be visible when using a non-soluble gas.

The trend of velocity in the experiment performed with CO_2 at 56 bars is very similar to that observed at 32 bars (see Figure 6(b)). This can be explained by the fact that solubility isopleths of CO_2 hardly increases with pressure at operating temperature (see for instance P-T diagram for CO_2 solubility by [28]). This indicates that similar gradients of density are expected at saturated and supersaturated conditions.

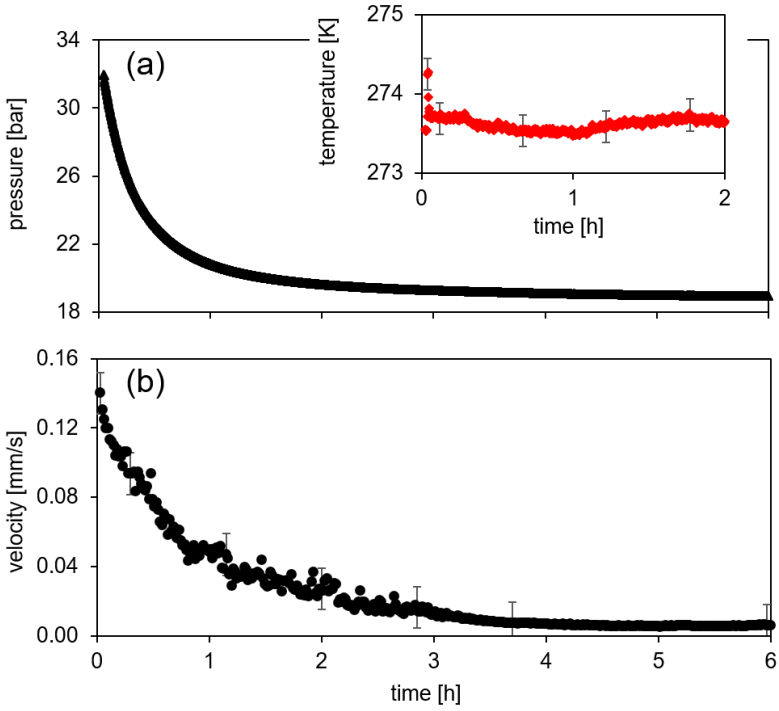

Figure 6. Pressure (a) and averaged velocity in the bulk of water (b) as a function of time. The inset depicts the temperature as a function of time. Experiment performed with 7 mL of water and CO_2 at 36 bars and 273.5 K.

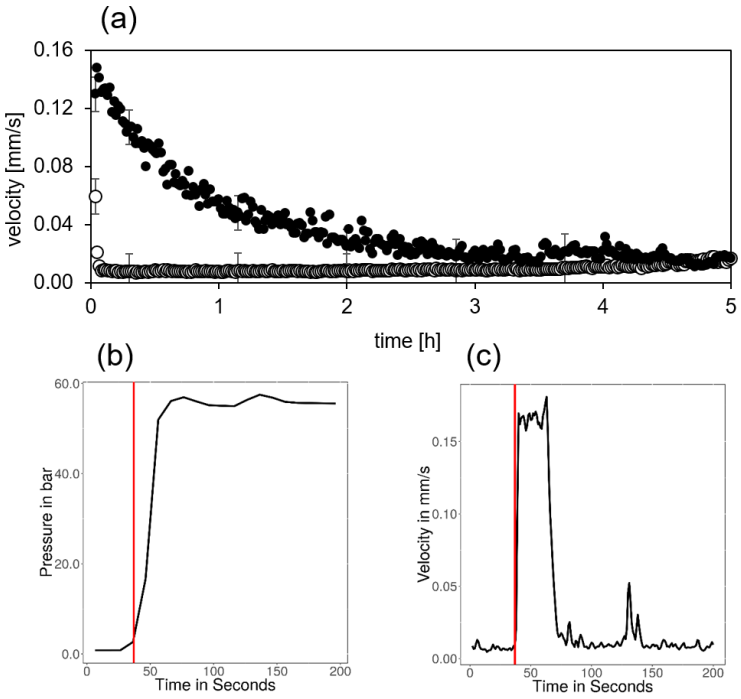

Figure 7. Averaged velocity in the bulk of water as a function of time (a). Solid and open symbols represent experiments performed with CO_2 and He, respectively. Experiments performed with 7 mL of water at 56 bar and 273.5 K. Pressure (b) and averaged velocity (c) right after increase of pressure for the experiment conducted with He.

3.3. Flow velocity measurements during GH formation

We performed a total of 45 experiments using SPS-5 as tracers for measuring the flow velocity in the bulk of water before and during the hydrate formation. From all 45 experiments, in 26 of them, the hydrate grew in the optical cell in less than 48 h. In what follows, we refer to those experiments as successful. For sake of feasibility, we stopped those experiments in which hydrate did not grow after 48 hours. In all of the successful experiments, independently of the volume of water used, i.e. 5.5 or 7 mL, and independently of the pressure selected, i.e. 36 or 56 bar, the initial nucleation occurred at the interface with inductions times ranging between 15 min and 45 hours. Under our experimental conditions, therefore, we could not find any significant effect of the pressure, or of the volume of water selected on the induction time.

Figure 8 depicts the snapshots for two different successful experiments performed with 7 mL of water at saturated conditions. Under the same conditions, the induction time was approximately 15 min (a)-(d) and 2 hours and 31 min (e)-(h), respectively. In both cases, a thin hydrate layer of about 0.5 mm (see Figure 4(d)) is formed first at the interface and we observe gas bubbles rising from the interface (see Figure 8(b) and (f)). This release of bubbles was only noticed when there is both a gas and a liquid CO_2 phase present. We hypothesize this phenomenon is driven by the heat supplied by the exothermic GH formation or due to the decrease of equilibrium CO_2 concentration in water with hydrate formation [29]. In experiments under saturated conditions, the sudden release of bubbles was used as a clear indication for the onset of hydrate formation.

Interestingly, the growth rate velocity between both experiments is completely different. In the experiment with a long induction time, we observed a rapid hydrate growth toward the bulk of water. After 2 seconds, the hydrate layer has covered a large portion of the water (Figure 8(g)) and after 6

seconds most the hydrate has grown throughout the reactor and there seems to be no water left (Figure 8(h)). On the other hand, in the experiment with a short induction time, the hydrate growth rate is much slower. After 2 seconds, the hydrate layer has barely increased (Figure 8(c)) and it requires about 23 min to cover completely the bulk of water (Figure 8(d)). This pattern in growth rate was observed in all experiments with an induction time lower than 30 minutes. Those experiments that took longer resulted in a rapid growth. This fact is directly related to how fast CO_2 is dissolved into water, which in turns is strongly influenced by the Rayleigh convection.

To clarify this point, Figure 9(e) illustrates the averaged velocity in the bulk of water as a function of time for the experiment depicted in Figure 5(a)-(d), blue triangles, and for the experiment depicted in Figure 8(a)-(d), red squares, respectively. The former corresponds to a long induction time experiment, 2 hours and 23 minutes, with the corresponding rapid growth pattern while the latter is an example of short induction time experiment with a much slower growth rate velocity. For sake of comparison, the averaged velocity of the experiment depicted in Figure 6 is shown in the figure, see black circles. In that case, no hydrate was formed during the first 6 hours. All the experiments were performed at saturated conditions, i.e. 56 bar and 237.5 K.

As shown in Figure 9(e), the long induction time example, blue triangles, presents a steeper slope on the initial stage of the averaged velocity as compared to the other two cases. This may be explained by the smaller volume of water used in this case, 5.5 mL instead of 7 mL. A faster distribution of CO_2 is therefore expected in the bulk of water. The final averaged velocity, however, achieves a similar final value than the experiment performed with 7 mL. The hydrate nucleation occurred after 140 minutes when the flow velocity is strongly diminished, indicating that convection currents due to CO_2 concentration gradients have been dropped and CO_2 is well distributed in the bulk of water. This fact explains the immediate growth of hydrate after nucleation which covered the entire bulk of water within a couple of seconds. Figures 9(c) and (d) depict the contour of velocity in the bulk of water 30 seconds before nucleation, and at onset of nucleation, respectively. The latter corresponds to the velocity profile of the snapshot depicted in Figure 5(a). The velocity seems to be higher in the left half of the water volume, just below the left side of the interface where hydrate grew (see Figure 5(a)). This may indicate that this increase of velocity is driven by the rapid hydrate crystallization.

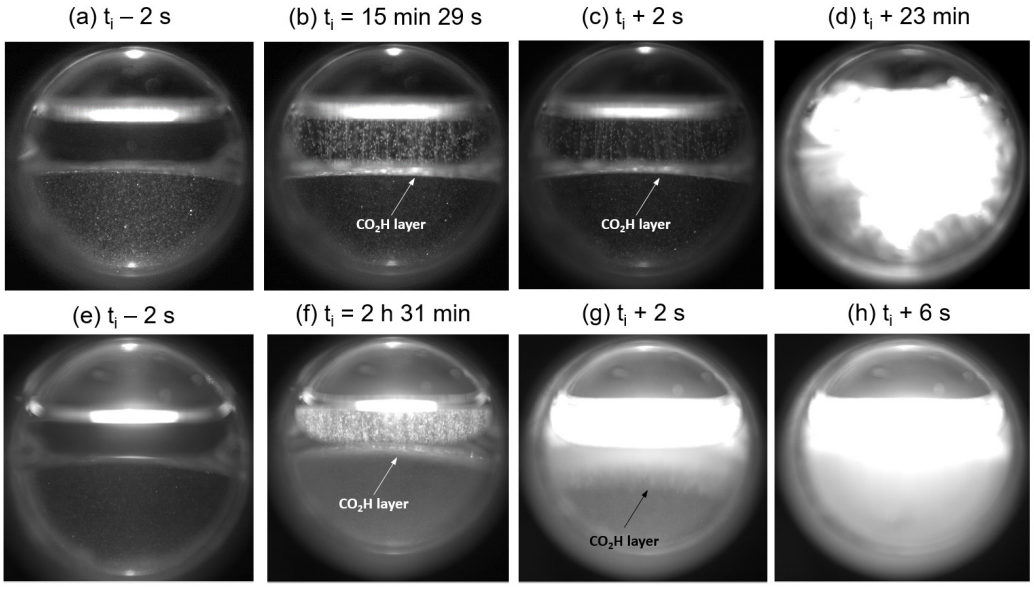

Figure 8. Snapshots illustrating the CO_2H formation for short (a)-(d) and long induction time experiments (e)-(g). Experiments performed with 7 mL of water and CO_2 at 36 bars and 273.5 K.

As expected, the averaged velocity in the short induction time experiment, red squares, presents a similar initial trend that the trial where non-hydrate was growth during the first six hours, black circles. The nucleation happened after about 15 min when the flow velocity is still very high indicating that convection currents are still present due to the gradient of CO_2 concentration. After this short period of time, there simply is not enough CO_2 dissolved in the whole water to sustain growth beyond a thin layer at the interface. The hydrate growth apparently becomes mass-transfer limited with a much lower growth rate velocity. We hypothesize that there should be a specific time threshold at which the concentration quickly changes to a sufficient level of CO_2 concentration. Before this point has been reached only the thin diffusion layer contains enough CO_2 to form hydrate, while shortly afterward the whole of the water can be transformed. The characteristic time for that threshold is dependent on how fast the CO_2 is dissolved in water and should be therefore dependent on the Rayleigh number. In our experiments, the threshold time was found to be 30 min.

Interestingly, the curve of averaged velocity shows a significant drop right after hydrate nucleates. For this kind of low induction lag experiments, PIV can be done continuously throughout nucleation and hydrate growth. Similar drops of velocity were observed right after nucleation in all the experiments with a short induction time. The dramatic drop in velocity can be also clearly discerned from the contour of velocity 30 second before nucleation, Figure 9(a), and at onset of nucleation, Figure 9(b). We consider two explanation for this phenomenon so far. One the one hand, the hydrate layer formed at the water-former interface is impermeable to gas transport as stated by [30], resulting in a sudden stop of Rayleigh convection. Secondly, the freezing in velocity could be due to the initial formation and agglomeration of labile cluster resulting into an increase of macroscopic viscosity. At this stage of research, more experiments are necessary to corroborate this hypothesis.

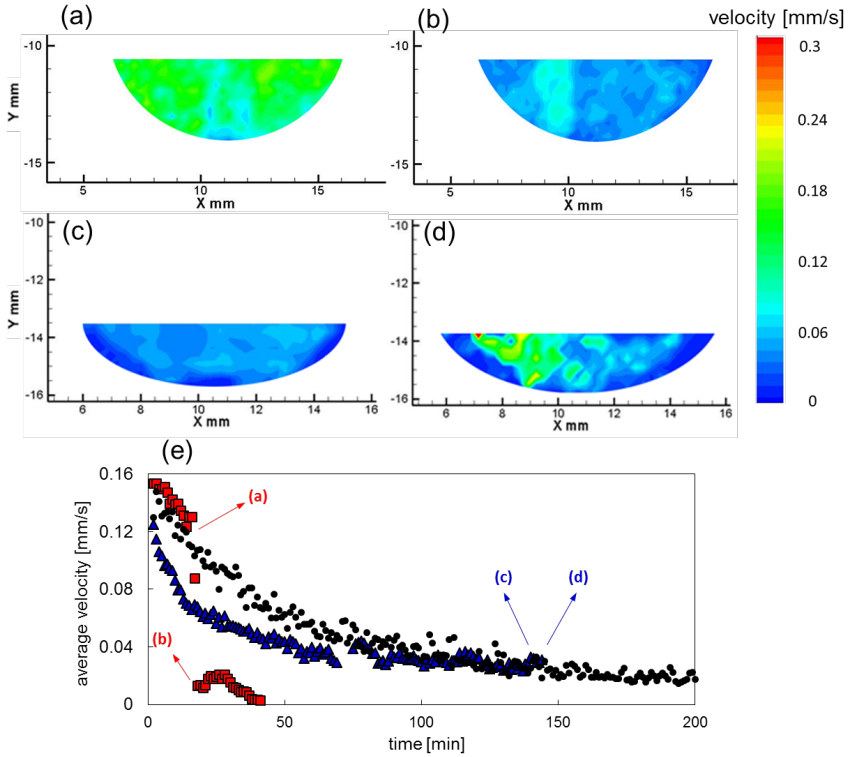

Figure 9. Contour of instantaneous flow velocity for a short induction time experiment 30 seconds before nucleation (a), at onset of nucleation (b) and for a long induction time experiment 30 seconds before nucleation (c) and at onset of nucleation (d). Averaged velocity over time (e). Red squares and blue triangles represent the short and long induction time experiment, respectively. Black circles represent an experiment in which hydrate did not grow over the first six hours.

4. Conclusions

We characterize the flow velocity field of the bulk of water during CO_2 hydrate formation in an optical cell with a volume of 12 mL filled with 5.5 or 7 mL of deionized water. For that purpose, two different imaging systems are simultaneously used for recording the particle-image fields from the front and the back, respectively. Classical particle image velocimetry (PIV) analysis is performed to obtain the map of velocity vectors. The system on the back, with a higher spatial resolution, is used to focus on the interface where hydrate is expected to form. The system from the front is used to analyze the velocity on the entire bulk of water. We first study the impact of tracers on the CO_2 hydrate formation. Glass spheres of 10 μm seem to act as nucleation spots resulting into a much faster hydrate formation in the bulk of water. Polyamide seeding particles of 5μm, however, displayed little effect on the hydrate growth process and are therefore deemed acceptable as tracer particles. Recirculation flows are noticed as a consequence of density-driven natural convection. We observe a gradual decrease of the averaged velocity with time as a consequence of this phenomenon. We performed a total of 45 experiments varying the volume of water and the pressure of the system, 36 and 56 bar, while the temperature was kept at 273.5 ± 0.5 K. Under those conditions, 26 of the experiments resulted in hydrate formation in less than 48 hours. The induction time varied widely between 15 min and 45 hours in those experiments. Hydrate was nucleate always at the interface. We could not recognize any significant impact of pressure or volume of water on the induction time. However, we identified two well-differentiated hydrate growth patterns depending on the hydrate induction time and the corresponding flow velocity on the bulk of water at that moment. The flow velocity depends on the CO_2 concentration distribution inside water due to Rayleigh convection phenomenon. For induction times above 30 min, CO_2 can be provided from the water phase resulting in rapid growth. Induction times below 30 min resulted in slow growth at the interface creating a solid barrier accompanied by a significant drop in the flow velocity.

References

[1] Sloan E D and Koh A C 2008 *Clathrate Hydrates of Natural Gases* (New York: CRC Press)
[2] Khan M R 2011 *Advances in clean hydrocarbon fuel processing: Science and technology* (Cambridge: Woodhead Publishing Limited)
[3] Matsumoto R, Ryu B J, Lee S R, Lin S, Wu S, Sain K, Pecher I, Riedel M 2011 *Mar. Petrol. Geol.* **28** 1751
[4] Max N D, Johnson A H and Dillon W P 2006 *Economic Geology of Natural Gas Hydrate* (Dordrecht: Springer)
[5] Brewer P G, Friederich G, Peltzer E T and Orr Jr F M 1999 *Science* **284** 943
[6] Genov G, Falenty A and Kuhs *The possible role of CO_2 hydrates for terra-forming processes on Mars (European Geosciences Union 2005)* **7** 05532
[7] Pellenbarg R E, Max M D and Clifford S M 2003 *J. Geophys. Res.* **108** E4 2156
[8] Yang M, Song Y, Ruan X, Liu L, Zhao J and Li Q 2012 *Energies* **5** 925
[9] Castellani B, Filipponi M, Nicolini A, Cotana F and Rossi F 2013 J*ournal of Energy and Power Engineering* **7** 883
[10] Kikkinides E S, Yang R T and Cho S H 1993 *Ind. Eng. Chem.* **32** 2714
[11] Scondo A and Sinquin A 2011 *Effect of additives on CO_2 capture from simulated flue gas by hydrates formation in emulsion 7th International Conference on Gas Hydrates*, Edinburgh, Scotland, UK
[12] Babu, P, Linga, P, Kumar, R, Englezos P 2015 *Energy* **85** 261-279
[13] Sivaraman, R 2003 *Gas TIPS News Letter* Fall 2003 Gas Technology Inst
[14] Park, K, Hong, S Y, Lee, J W, Kang, K C, Lee, Y C, Ha M G, Lee, J D 2011 *Desalination* **274** 91-96
[15] Babu, P, Kumar, R, Linga, P 2014 *Desalination* **274** 91-96
[16] Kang, K C, Linga, P, Park, K, Choi, S J, Lee, J D 2014 *Desalination* **353** 84-90

[17] Li, S, Shen, Y, Dongbing, L, Fan, L, Zhang, Z, Li, W 2014 *Advance Journal of Food Science and Technology* Bd **6 6** 780-783
[18] Li, S, Shen, Y, Dongbing, L, Fan, L, Tan, Z 2015 *Chemical Engineering Research and Design* **93** 773-778
[19] Farajzadeh, R, Hamidreza, S, Zitha, P L J, Bruining, H 2007 *Int. J. Heat Mass Transfer* **50** 5054-5064
[20] Farajzadeh, S, Zitha, P L J, Bruining, H 2009 *Ind. Eng. Chem. Res*. **48** 6423-6431
[21] Khosrokhavar, R, Elsinga, G, Farajzadeh, R, Bruining H 2014 *J. Pet. Sci. Eng.* **122** 230-329
[22] Agudo J R and Wierschem A 2012 *Phys. Fluids.* **093302** 24
[23] Agudo J R, Dasilva S and Wierschem A 2014 *Phys. Fluids.* **053303** 26
[24] Gmelin, L 1973 **8** Auflage Kohlenstoff Teil C3 Verbindungen
[25] Mohammadi A, Manteghian M, Haghtalab A, Mohammadi A H, Rahmati-Abkenar M 2014 *Chemical Engineering Journal* **237** 387395
[26] Nesterov A, Reshetnikov A, Manakov A Y, Rodionova T, Pauk-shtis E, Asanov I, Bardakhanov S, Bulavchenko A 2015 *Journal of Molecular Liquids* **204** 118125
[27] Lirio C. F. S, Pessoa F L P and Uller A M C 2013 *Chem. Eng. Sci.* **96** 118123
[28] Diamond, W L, Akinfiev, N N 2003 *Fluid Phase Equilibria* **208** 265-290
[29] Ohmura R, Shimada W, Uchida T, Mori Y H, Takeya S, Nagao J, Minagawa H, Ebinuma T and Narita H 2014 *Philosophical Magazine* **84** (1) 116
[30] Sun C, Peng B, Dandekar A, Ma Q and Chen G 2010 *Annual Reports Section "C"* (*Physical Chemistry*) **106** 77100